Sustainable Structures
ISSN: 2789-3111 (Print); ISSN: 2789-312X (Online)
http://www.sustain-dpl.com/journal/sust
DOI: 10.54113/j.sust.2026.000100

ORIGINAL ARTICLE

Load-bearing performance of laminated bamboo lumber-steel plate single-bolt connections

Jingwen Su[a], Yukun Tian[b], Yijia Guo [c], Haitao Li[b*], Zhenhua Xiong[d], Usama Sayed[b], Gensheng Cheng[b], Rodolfo Lorenzo [e]

[a] Nanjing Technical Vocational College, Nanjing 210019, China
[b] College of Civil Engineering, Nanjing Forestry University, Nanjing 210037, China
[c] School of International Education, Tianjin Chengjian University, Tianjin 300384, China
[d] Ganzhou Sentai bamboo company LTD, Ganzhou 341001, China
[e] University College London, London WC1E 6BT, UK
*Corresponding author: Haitao Li, Professor, E-mail: lhaitao1982@126.com

Abstract: In order to investigate the mechanical properties of laminated bamboo lumber-steel plate bolted connections under compression parallel to grain, a series of tests has been carried on considering the diameter of the bolts, the thickness of the main component and the end spacing of the bolts. The failure mode, stiffness, bearing capacity and ductility ratio of the connections were studied considering the influencing factors. The test results show that the failure mode gradually changes from brittle shear failure to ductile yield failure with the increasing of the thick-to-diameter ratio. As the diameter of the bolt increased, the stiffness and load of the connections increased gradually, but the ductility ratio did not change after the diameter reached about 16 mm. The initial stiffness of the connections reached the maximum value at 125 mm thickness of the main component. The yield load and ultimate load no longer showed a significant increasing trend after the thickness reached 100mm, and the ductility ratio was less affected by the thickness of the main component than by the diameter. The end spacing of the bolts had no significant effect on the load-bearing performance of the connections compared to the bolt diameter and the thickness of the main component. Based on the test results comparing the current national wood structure design standards, the American standards are more conservative, while the Chinese and European standards are in good agreement with the test. Considering the bolt diameter and the main component's thickness as the main influencing factors, the load-bearing formula was proposed and it could give a reference for calculating the bearing capacity of laminated bamboo lumber-steel plate single-bolt connection.

Keywords: laminated bamboo lumber, steel plate bolt connection, failure mode, load bearing calculation

1 Introduction

Green building materials have attracted more and more attention from both scientists and engineers. Bamboo structures are a type of green building [1-3]. However, due to the unstable mechanical properties of the raw bamboo material itself and the large shape and size restrictions which make bamboo structures have great limitations [4-6]. They need to be processed to meet the requirements of

Received: 24 November 2024; Received in revised form: 4 August 2025; Accepted: 29 August 2025

modern building structure materials, and these needs promote the emergence of engineered bamboo materials. There are three types of engineered bamboo materials commonly used as bamboo structural materials laminated bamboo lumber (LBL), parallel bamboo strand lumber (PBSL) and glued bamboo weaving materials. Performance tests on LBL show that the material has great potential for application [7-13]. Through experimental research, it can be applied to beams and columns of building structures, solving the technical problem of bamboo structures requiring large cross-sectional size members [14-23]. **Fig. 1** shows two typical LBL projects.

(a) Indian airport

(a) Building of Sentai Bamboo Research Center [3]

Fig. 1. Engineering applications of LBL

Connections failure is common in bamboo structures [24-25]. Trayer proposed that the damage form and load capacity of bolted connections were influenced by the member's edge, middle, and end distances [26]. Jonhansen proposed the theory of yielding of pin grooves and bolts in wood and derived the calculation method for bolted connections [27]. McLain et al. [28] and Soltis et al. [29] validated the applicability of European Yield Model and perfected it to determine the yield strength of the connector within a specific precision range. The concept of effective bolts was proposed by N. Gattesco in an experimental study of multi-bolt steel-wood nodes [30]. Later, César studied the effect of different end distances and bolt diameters on the performance of single bolt connections [31] Bolted connections are now widely used in modern wood structures [32-36]. Some progress has also been made in the study of the bolting of bamboo materials. Reynolds et al. found significant differences in the mechanical properties of bolted nodes on wood structures and bamboo composite materials, with most of the bolted nodes on bamboo composite materials breaking at the maximum shear stress [37]. Zhou analyzed the effect of different side material thicknesses and bolt end distances on the tensile load-bearing performance of reconstituted bamboo-steel infill plates bolted to the smooth grain [38]. Khoshbakht et al. found that the damaged region of the Laminated Veneer Bamboo dowel connections had deviated from the center of the bolt-bamboo contact, controlled by the ratio of shear stress to shear strength [39]. Cui et al. studied the effect of factors such as thickness to diameter ratio and end distance on the tensile properties of bolted steel-psb-steel connections and summarized their damage forms [40]. Li et al. studied the performance of scrimber bamboo steel cleat bolted connections and derived the theoretical calculation formulae suitable for the bearing strength of parallel bamboo strand lumber pin grooves and steel cleat bolted connections [41]. As discussed above, many scholars have conducted numerous studies on the load-bearing properties of wood as well as some studies on the parallel bamboo strand lumber bolted connections.

As for laminated bamboo lumber-steel plate bolted connections, the related research is limit. More studies are needed about it in order to promote its application in engineering. Thus, considering the diameter of the bolts, the thickness of the main component and the end spacing of the bolts, the specimens were designed and the related tests were carried on under compression parallel to grain. Detailed discussion about the mechanical properties of the connections were done in this paper based on the test results. Comparisons among different national standards were conducted and a new formula to calculate the bearing capacity of the connections was proposed.

2 Materials and Methods

2.1 Test material

Fig.2 shows the manufacturing process of the laminated bamboo lumber. All test specimens used in this paper were all produced by Ganzhou Sentai bamboo company LTD. As for the compression test, 20 specimens were designed with the cross-section of 50 mm × 50 mm, and the height of 100 mm. The moisture content measured during the test was about 9%, the density was 0.672 g/cm^3, and the compressive strength parallel to grain was 71.95 MPa. The steel plate was made of Q345 steel, and the thickness is 10 mm. The diameter of the hole in the steel plate is 1.5 mm larger than the diameter of the corresponding bolt. The material used for the bolts was Q235 grade steel, and the flexural yield strength was measured at 624.5 MPa, 598.5 MPa, 565.1 MPa, 642.1 MPa, and 693.4 MPa for bolts with diameters of 12 mm, 14 mm, 16 mm, 18 mm and 20 mm, respectively, referring to the test method of ASTM F1575 [42]. The screw length of the bolt is the sum of the thickness of the main component and the two steel plates and was designed to avoid shear damage to the connection at the junction of the light and threaded rod of the bolt during the load-bearing process.

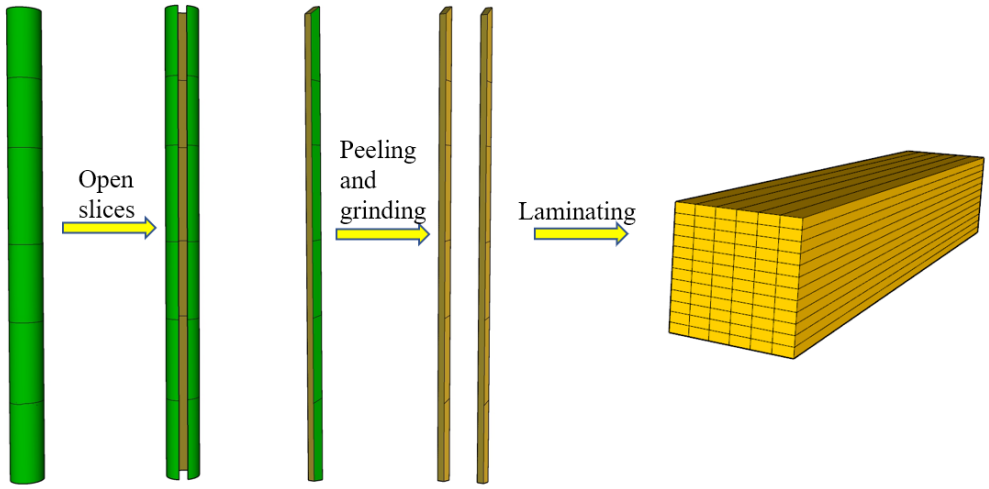

Fig. 2. Laminated bamboo lumber manufacturing process

According to ASTM D5764-97a test method, the half-hole pin groove bearing test was conducted on laminated bamboo lumber, as illustrated in **Fig. 3**, and the test results are shown in **Table. 1.**

Fig. 3. The half-hole pin groove bearing test of laminated bamboo lumber

Table. 1. Compressive strength of the LBL half-hole pin slot

Number	Bolt diameter	Number of specimens	Average value /MPa	C.V./%
1	12	10	84.48	8.02
2	14	10	80.57	6.74
3	16	10	77	6.52
4	18	10	77.75	4.45
5	20	10	72.08	7.02

2.2 Test program and loading system

Table. 2. Parameters of single-bolt connection specimens of LBL-steel plate in each group

Group		Bolt diameter (mm)	End distance (mm)	Thickness of LBL (mm)	Number
ZCSBD	ZCSBD12	12	64	100	5
	ZCSBD14	14	64	100	5
	ZCSBD16	16	64	100	5
	ZCSBD18	18	64	100	5
	ZCSBD20	20	64	100	5
ZCSBE	ZCSBE36	12	36	100	5
	ZCSBE48	12	48	100	5
	ZCSBE60	12	60	100	5
ZCSBT	ZCSBT50	12	48	50	5
	ZCSBT75	12	48	75	5
	ZCSBT100	12	48	100	5
	ZCSBT125	12	48	125	5
	ZCSBT150	12	48	150	5

In order to study the mechanical performance of the single bolt connection of LBL-steel plate, the bolt diameter, the thickness of the main component, and the end spacing were selected as the influencing factors to design the test specimens. The length of all laminated bamboo lumber is 150mm. Numbering of the specimens, ZCSB indicated the single bolt connection specimen with paralleling compression, D indicated the diameter; E indicated the end distance; T indicated the thickness of the main member. For example, ZCSBD indicates the group of specimens with different diameters in the paralleling compression direction. The design parameters of each group of specimens are shown in **Table. 2.**

The main components and loading device diagram of the main LBL specimen is shown in **Fig. 4**.

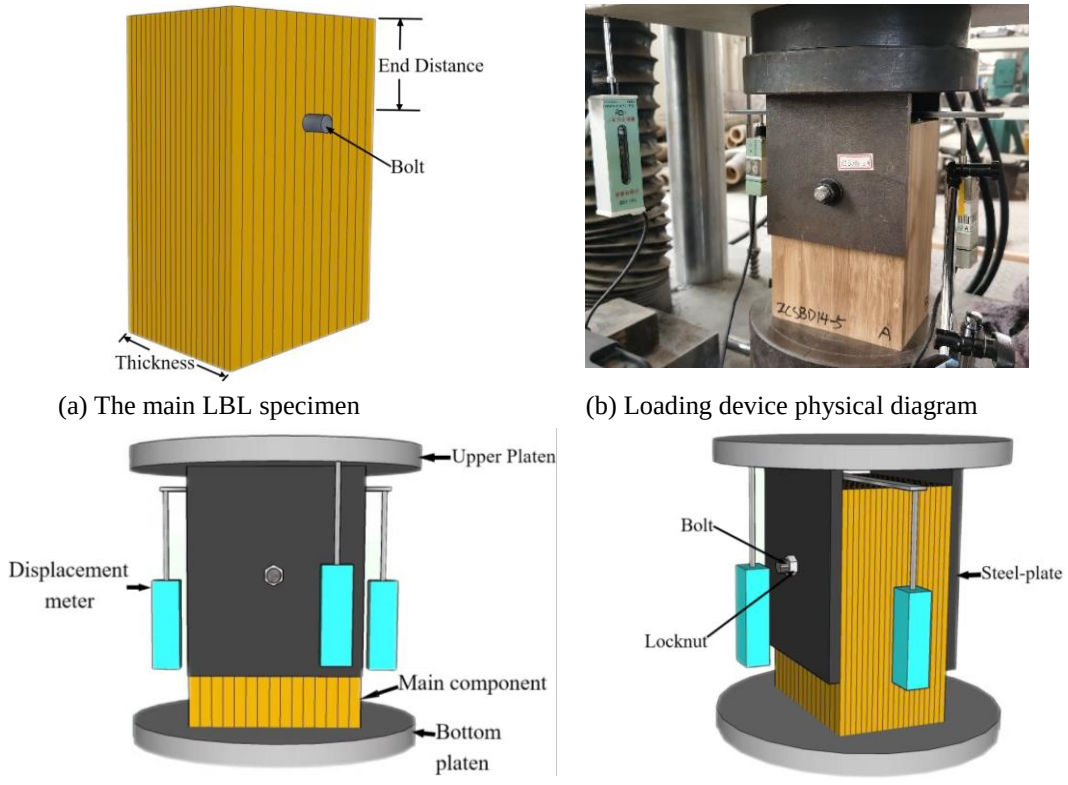

(a) The main LBL specimen (b) Loading device physical diagram

(c) Front view of loading device (d) Side view of loading device

Fig. 4. Main components and loading device diagram

200t microcomputer control electro-hydraulic servo universal testing machine and TDS-530 data acquisition system were chosen for the loading tests. Four faces of the main component were named in counterclockwise order as face A, face B, face C, and face D.

Assembled each group of main components and corresponding steel plates into single-bolt double-

shear connection members through bolts, and the connections were tightened with wrenches to prevent slippage of the steel plates during the loading process. A slender steel piece with sufficient weight was glued above the main component (the weight is sufficient to ensure that no vibration occurred during the loading of the specimen), and a displacement meter was arranged below each end of the steel piece for measuring the vertical displacement of the main component at the left and right ends, respectively. Then a displacement meter was arranged under the upper platen to measure the displacement of the steel clamping plate. Detailed test setup could be seen from **Fig. 4.** The loading speed for all tests was 1.5 mm/min.

3 Experimental phenomena and damage models

Fig. 5 shows three main failure modes for LBL-steel plate bolted connections according to the test results.

Mode I: Shear damage. Shear damage occurred for the LBL parts due to insufficient bonding between the bamboo pieces. None deformation could be seen in the bolts and test pieces had obvious cleavage cracks.

Mode II: One-hinged yielding damage. Damage to the main component was caused by insufficient bearing capacity of the LBL pin slot. One hinge appeared in the bolt and both ends of the steel were straight without obvious bending.

Mode III: Two-hinged yielding damage. The bolt was bent due to excessive extrusion deformation of the pin slot below the hole of the bamboo bolt, and the bolt was sheared and damaged by the joint action of tension and shear. **Figs. 5, 6 and 7** show the damage photos of the series of typical specimens and the damage modes to which they belong.

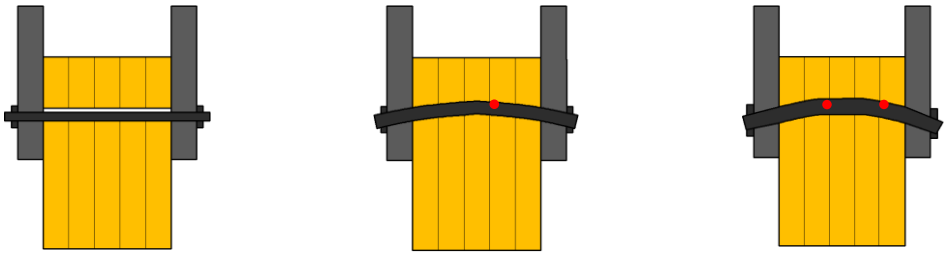

(a) Mode I shear damage (b) Mode II one-hinged yielding (c) Mode III two -hinged yielding

Fig. 5. Yield mode of steel plate bolted connections

As can be seen from **Fig. 6a**, the damage for the ZCSBD12 series specimen belong to mode III, i.e. the bolt appeared to have two plastic hinges. No significant changes in the specimen at the beginning of the loading. Slippage occurred between the steel clamp and the LBL parts as the load increased. With continuing increasing of the load, the bolt yielded and two plastic hinges appeared. Due to two plastic hinge parts of the bolt tilt bending, the extrusion occurred in face A and C of the main component and the bent part of the bolt embedded in the main component. The bolt yielded and the bolt bending degree was obvious. The lower part of the bolt hole of the main component had obvious deformation caused by the embedding of the bolt, and the surface did not have obvious cracks generated. No deformation could be seen in the steel plate.

Fig. 6b shows the failure mode for ZCSBD14 series specimens and it belongs to damage mode III. The previous phenomenon was the same as ZCSBD12 series specimens, but with the increase of load, the bolts of some specimens appeared two plastic hinges, while some specimens appeared with only one plastic hinge or two plastic hinges without a clear boundary. Penetration cracks along the glue line appeared in some of the LBL components due to insufficient bonding of the bamboo layer before the bolt yielding. The bolt bending degree was more obvious. The lower part of the bolt hole of the main component had obvious deformation caused by the embedded bolts, and the steel plate had no obvious deformation. The failure modes for ZCSBD16 and ZCSBD 18 series specimens could be seen in **Fig. 6c** and **Fig. 6d**. They belong to damaged mode II. The final bolt was sheared and damaged, and the bolt was bent to a more significant degree. Among them, the main component for ZCSBD16-5 had cracks caused by the cracking of the glue layer, and no obvious deformation could be seen for the bolts.

Although only one plastic hinge appears for ZCSBD16 and 18 series bolts, the bending degree of the bolt gradually decreased as the bolt diameter increased. **Fig. 6e** shows failure mode for ZCSBD20 series which also belongs to damage mode II, however the plastic hinge is not obvious.

As discussed above, the effect of bolt diameter size on the damage mode of LBL-steel plate bolted connections could be summarized as following. Yield failure with two plastic hinges in the bolts happened in the connections with the bolt diameters of 12 and 14 mm. with the increasing of the bolt diameter, the damage mode with only one plastic hinge appeared when the bolt yielded. As for the bolt with the diameter of 20 mm, no significant yield damage occurred and shear damage occurred for the main component of some specimens. Thus, as the bolt diameter increased, the damage mode of the connections developed from the bolt plastic yield damage gradually to shear damage of the main component but the bolt did not yield.

(a) ZCSBD12: damage mode III (b) ZCSBD14: damage mode III

(c) ZCSBD16: damage mode II (d) ZCSBD18: damage mode II

(e) ZCSBD20: damage mode II

Fig. 6. Damage mode of connections with different diameters

The failure mode for ZCSBT50 series specimen belongs to shear damage of the main component, as illustrated in **Fig. 7a.** Splitting along the bolt hole occurred through the entire main component but the bolt did not yield. And the bolt had slight bending but no obvious plastic hinge appeared. Bolt yielding occurred for ZCSBT75 series specimen and the damage mode with one plastic hinge belongs to mode II, as illustrated in **Fig. 7b.** The main LBL component only had the deformation caused by the bolt extrusion of the bolt hole. The bolt hole was crushed and no crack appeared as a whole. **Fig. 7c, Fig. 7d, Fig. 74** show the failure phenomenon for ZCSBT100, ZCSBT125 and ZCSBT150 respectively. As the thickness of the main component increased, the distance between the two plastic hinges increased and closed to the edge of the main component gradually. No damage occurred to the main LBL component. This showed the effect of the thickness of the main component on the damage mode. When

the thickness of the main component was small, the bolt did not yield, and the main component was damaged by the bolt shear. With the increased thickness of the main component, the plastic hinge of the bolt appeared, and the distance between the two plastic hinges increased with the increase in the thickness of the main component. No significant damage to the main component occurred when the bolt yielded.




(a) ZCSBT50：damage mode I (b) ZCSBT75：damage mode II




(c) ZCSBT100：damage mode III (d) ZCSBT125：damage mode III


(e) ZCSBT150：damage mode III

Fig. 7. Damage mode of connections with different Thickness of main components




(a) ZCSBE36：damage mode III (b) ZCSBE60：damage mode III

Fig. 8. Damage mode of nodes with different Bolt end distance

Fig. 8 shows the failure photos for the specimens with different bolt end distances**.** The damage modes of the bolts with different end distances were all Mode III. The bolts were yielded and two plastic

hinges appeared. However the damage mode was not significantly affected by the end distance size. No significant damage to any of the main components.

In summary, the damage mode of LBL-steel plate bolted connections are mainly related to the bolt diameter and the thickness of the main component, while the bolt end distance has little effect on it. Therefore, the thickness to diameter ratio (the LBL thickness/bolt diameter) is introduced, as shown in **Fig. 9**, to analyze the failure mode of the single bolt connection of LBL-steel plate. With the increase in thickness-to-diameter ratio, the damage mode of the LBL-steel plate connection gradually changes from brittle shear damage to ductile yielding damage with the appearance of multiple plastic hinges. Where 4.16 is the ratio for the specimen with the LBL thickness of 50 mm with the bolt diameter of 12 mm and 6.25 is the ratio for the specimen with the LBL thickness of 100 mm with the bolt diameter of 16 mm.

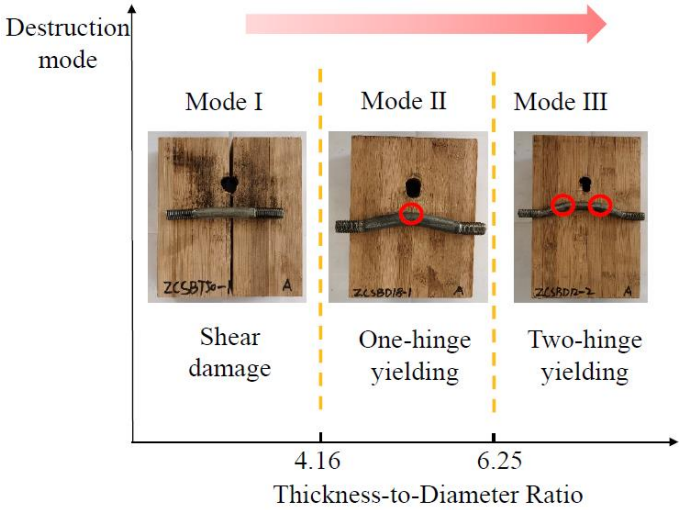

Fig. 9. Thickness to diameter ratio division of damage pattern type

4 Experimental results analysis

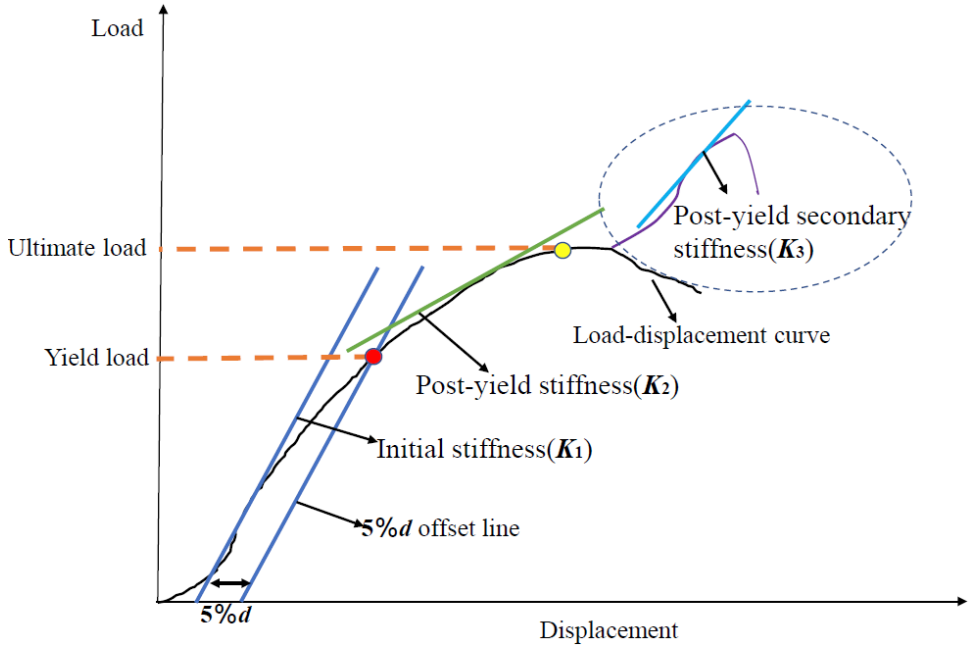

Fig. 10. The method for determining the bearing capacity of the connections

As shown in **Fig. 4** for the test setup. The displacement of the main LBL components measured by the displacement meter on the steel plate (the average of the displacements recorded by the

displacement meters on both sides) minus the displacement of the steel plate was the relative slip of the test specimen. Combined with the data measured by TDS, it was found that the maximum displacement of the main member was only 0.3mm, which was negligible compared with the displacement of the steel plate. Therefore, the load displacement curve of the steel plate was approximately the load slip curve of the bolted connections. **Fig. 10** shows the method for determining the bearing capacity of the connections. Firstly, the scale factor, named the initial stiffness K_1, could be obtained by fitting the load displacement of the linear elastic phase of the load-slip curve. The yield load and yield displacement of the specimen could be determined by referring to the 5% bolt diameter offset method as specified in ASTM D5764-97a. The post-yield stiffness K_2 is the resist deformation capacity of the connection under external forces after the load carrying capacity exceeds the yielding load of the connection. As can be seen the dotted box in **Fig. 10**, some specimens have a secondary reinforcement stage after reaching yield point discovered in the load-slip curve. The post-yield secondary stiffness K_3. Could be taken as the slope of the fitted line segment.

4.1 Effect of bolt diameter on node load-bearing performance

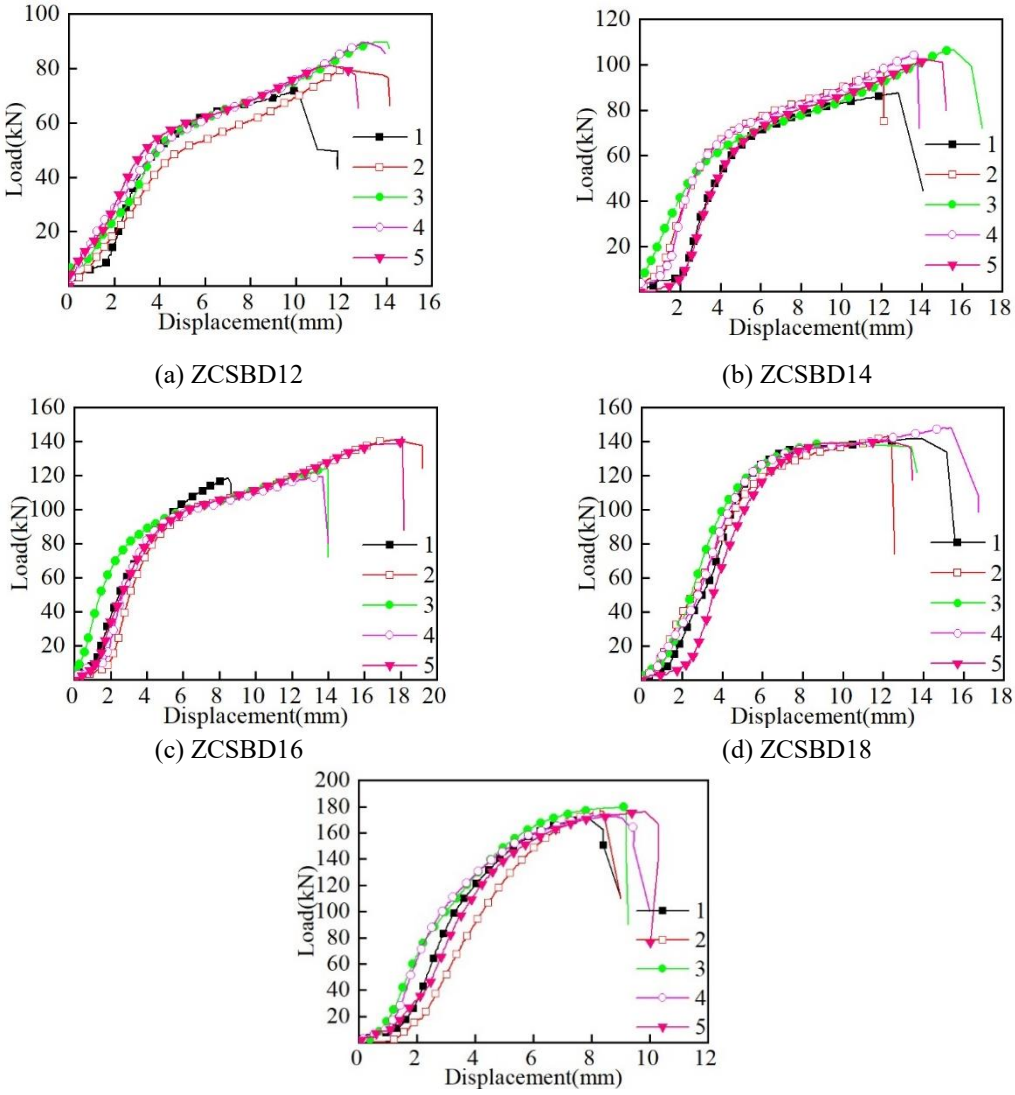

(a) ZCSBD12 (b) ZCSBD14

(c) ZCSBD16 (d) ZCSBD18

(e) ZCSBD20

Fig. 11. Load-slip curves of ZCSBD group

Fig. 11 shows the load-slip curves of ZCSBD group. At the beginning of the test, the bolt was not in complete contact with the bolt hole and could slide freely, so the load-slip curve has a small horizontal line in the early stage. With the load increasing, the bolt gradually contacted with the main component, and the load gradually increased linearly while the displacement increased slowly. As the load increased

gradually, the bolt was embedded into the main component gradually. The linear elastic phase ended, and the bolt entered the yielding phase. While the bolt gradually bent with the increase in load, the stiffness was significantly reduced, and there was an obvious yielding platform. After the yielding stage lasted for some time, there was a clear rise in the load-displacement curves of ZCSBD12, ZCSBD14, ZCSBD16 series specimens, and ZCSBD18-4. As the bolt was embedded in the LBL after bending to a certain extent, the bolt was subjected to the shear of the steel plate at both ends and the reverse binding force of the main component at the bottom. That was to say the bolt was under the combined of tension and shear and was subjected to secondary reinforcement. At this time, the displacement of the connections developed rapidly while the load developed slowly. At this point, the stiffness has increased compared to that in the yield stage, but it is significantly lower than the initial stiffness. However, no secondary reinforcement phenomenon appeared in most of the specimens of ZCSBD18 series and ZCSBD20 series. Due to the increase of the bolt diameter, the flexural bearing capacity and the ability to resist deformation increased gradually, and the specimen failed in shear. When the load reached the ultimate load point, the specimen was damaged and lost its bearing capacity. The bolt would not undergo secondary strengthening with the increase of the bolt diameter. The test results for ZCSBD group are shown in **Table. 3.**

Table. 3. Test results of ZCSBD group

Number	P_y (kN)	d_y (mm)	K_1 (kN/mm)	K_2 (kN/mm)	P_u (kN)	d_u (mm)	μ	K_3 (kN/mm)
ZCSBD12-1	60.32	5.49	24.1	3.23	73.28	11.84	2.15	—
ZCSBD12-2	68.48	9.83	12.61	3.63	82.88	14.24	1.44	5.48
ZCSBD12-3	89.76	13.43	12.98	3.63	89.76	14.12	1.05	5.01
ZCSBD12-4	88.8	12.77	11.78	4..13	89.6	14.38	1.12	5.33
ZCSBD12-5	54.88	3.98	18.13	5.5	81.12	12.77	3.2	5.01
Average	72.44	9.1	15.92	3.9975	83.32	13.47	1.8	5.2075
CV	19.89%	41.71%	29.26%	25.50%	7.33%	7.41%	44.82%	4.53%
ZCSBD14-1	75.68	7.21	31.65	4	87.84	14.07	1.95	—
ZCSBD14-2	83.84	7.95	27.69	3.69	97.44	12.08	1.52	4
ZCSBD14-3	90.4	11.6	18.96	3.42	106.56	16.46	1.41	3.74
ZCSBD14-4	91.04	10.52	35.93	3.79	104.48	20.79	1.97	4.28
ZCSBD14-5	74.88	6.44	30.25	3.23	102.08	15.03	2.33	3.79
Average	83.16	8.74	28.89	3.626	99.68	15.69	1.84	3.9525
CV	8.32%	22.65%	19.52%	8.39%	6.67%	18.63%	18.11%	6.21%
ZCSBD16-1	88.64	4.53	31.87	7.2	118.88	8.64	1.9	—
ZCSBD16-2	94.88	7.65	38.02	2.74	140.96	16.21	2.11	2.85
ZCSBD16-3	92.16	6.5	40.3	2.66	124.32	14.37	2.21	—
ZCSBD16-4	94.72	6.33	40.78	2.66	120.32	15.79	2.49	—
ZCSBD16-5	123.04	12.82	27.54	2.66	156.48	30.78	2.4	4
Average	98.68	6.57	35.7	3.584	132.19	17.16	2. 22	3.425
CV	12.55%	48.11%	14.48%	56.40%	10.95%	47.76%	10.55%	23.70%
ZCSBD18-1	130.72	6.46	34.7	2.4	142.08	15.15	2.34	—
ZCSBD18-2	126.24	7.02	41.16	4.8	144	12.4	1.76	—
ZCSBD18-3	121.6	5.49	43.85	4	139.52	13.68	2.49	—
ZCSBD18-4	134.88	7.69	41.61	4.5	148.32	16.75	2.17	4.69
ZCSBD18-5	118.72	6.12	40.7	4.8	140.32	13.47	2.2	—
Average	126.43	6.56	40.20	4.1	142.84	14.3	2.2	4.69
CV	4.65%	11.48%	8.42%	24.50%	2.20%	10.57%	11.07%	0.00%
ZCSBD20-1	139.36	4.81	60.24	17	171.52	8.4	1.74	—
ZCSBD20-2	158.72	6.55	41.93	12.8	176.8	8.4	1.28	—
ZCSBD20-3	129.92	4.1	55.49	13.7	179.84	9.19	2.23	—
ZCSBD20-4	133.28	4.21	61.14	13.96	173.76	9.45	2.24	—
ZCSBD20-5	151.52	5.71	50.28	15.2	176.32	10.29	1.8	—
Average	142.56	5.08	53.81	14.532	175.64	9.15	1.86	—
CV	7.67%	18.38%	13.18%	12.16%	1.61%	7.74%	19.25%	—

Note: *CV* is the the coefficient of variation, P_y is the yield load, P_u is the ultimate load, d_y is the yield displacement, d_u is the ultimate displacement, K_1 is the initial stiffness, K_2 is the secondary stiffness after yielding, μ the ductility ratio (d_u/d_y), K_3 is the stiffness of the secondary reinforcement of some specimens.

As can be seen from **Table. 3** and **Fig. 12a**, the initial stiffness K_1 of the bolt increased with the increased of the bolt diameter. The initial stiffness increased faster and by 81% when the diameter was increased from 12 mm to 14 mm. The initial stiffness increase decreased when the diameter increased to 18 mm. The most significant increase in initial stiffness was achieved when the bolt diameter was increased from 18 mm to 20 mm, with an increase of 33.85%. The coefficient of variation of the initial stiffness K_1 was larger only for 12 mm and 14 mm and was smaller for the other three groups. In addition, there was no significant difference between the specimens. In summary, the bolt diameter is positively correlated with the initial stiffness K_1. As for the stiffness K_2 after yielding, there was no significant increase when the diameter of the bolt increased from 12 mm to 18 mm. However, when the diameter of the bolt reached 20 mm, the yield strength of the bolt increased significantly at this time, with an increase of 253.65%. Since the 20 mm bolts did not yield at the end of the test, the stiffness at this point was significantly greater than the yield stiffness of the other groups of bolts, which showed that the 20 mm bolts were not fully utilized. For ZCSBD12, 14, and 16 series specimens with secondary reinforcement, $K3$ was basically comparable to the size of yield stiffness $K2$, and there was no significant increase in stiffness, and the slip had been increasing while the load was increasing more slowly.

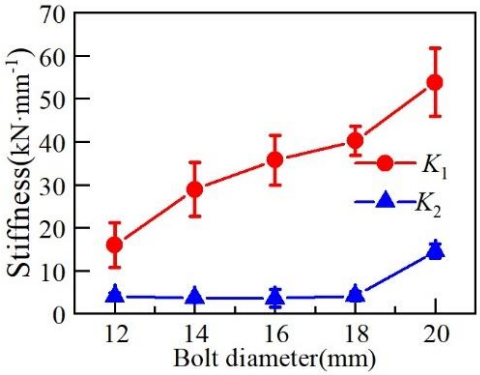

(a) Stiffness for different diameters

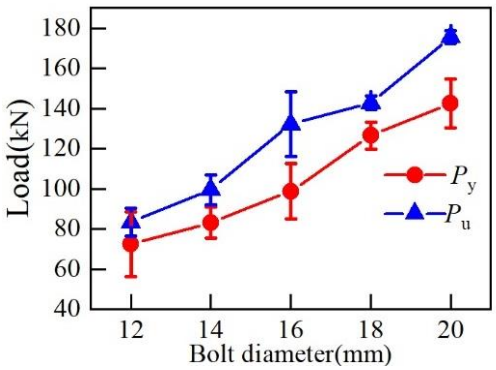

(b) Load for different diameters

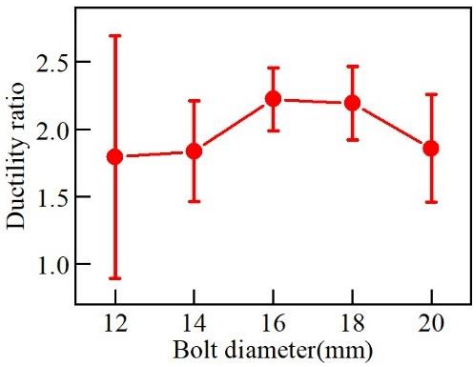

(c) Ductility ratios for different diameters

Fig. 12. Multiple comparisons of bolt diameters

As can be seen from **Fig. 12b**, the yield load and ultimate load corresponding to the connections with different bolt diameter increased linearly with the increase of bolt diameter. The yield load P_y and ultimate load P_u increased by 100.12 kN and 92.32 kN respectively, for ZCSBD20 compared to ZCSBD12. Only ZCSBD12 and ZCSBD16 series specimens have a large coefficient of variation, while other groups of specimens have no significant differences.

Fig. 12c shows the relationship between bolt diameter and ductility ratio**.** Among ZCSBD series, the highest ductility ratio is 2.2 for ZCSBD16 series, while the lowest is 1.8 for ZCSBD12 series. The ductility ratio for the ZCSBD12 and ZCSBD14 series specimens is kept at about 1.8 without significant changes, indicating that the bolt diameter does not affect the deformation resistance of the connection in this interval. When the bolt diameter increases to 16 or 18 mm, there is a slight increase in the ductility to about 2.2, and remains flat. This shows that when the bolt diameter increases to 16 mm, the bolt's ability to resist deformation after yielding increases, and the ductility becomes larger. As the main

component has undergone shear failure before the connection bolts reached the yield state, the deformation resistance capacity of the bolts has not been fully utilized. Therefore, the ductility rate of the ZCSBD20 node has dropped to around 1.8 again. Therefore, when the bolt diameter increased, the resistance of the connection to deformation would also increase. When the bolt diameter increased to 16 mm, the ductility of the connection would remain stable, and the resistance to deformation would be stronger. The connection ductility rate reached the maximum when the bolt was about 16~18 mm, and the load-bearing properties of the bolt and the main component were fully utilized at this time.

4.2 Effect of main member thickness on node load-bearing performance

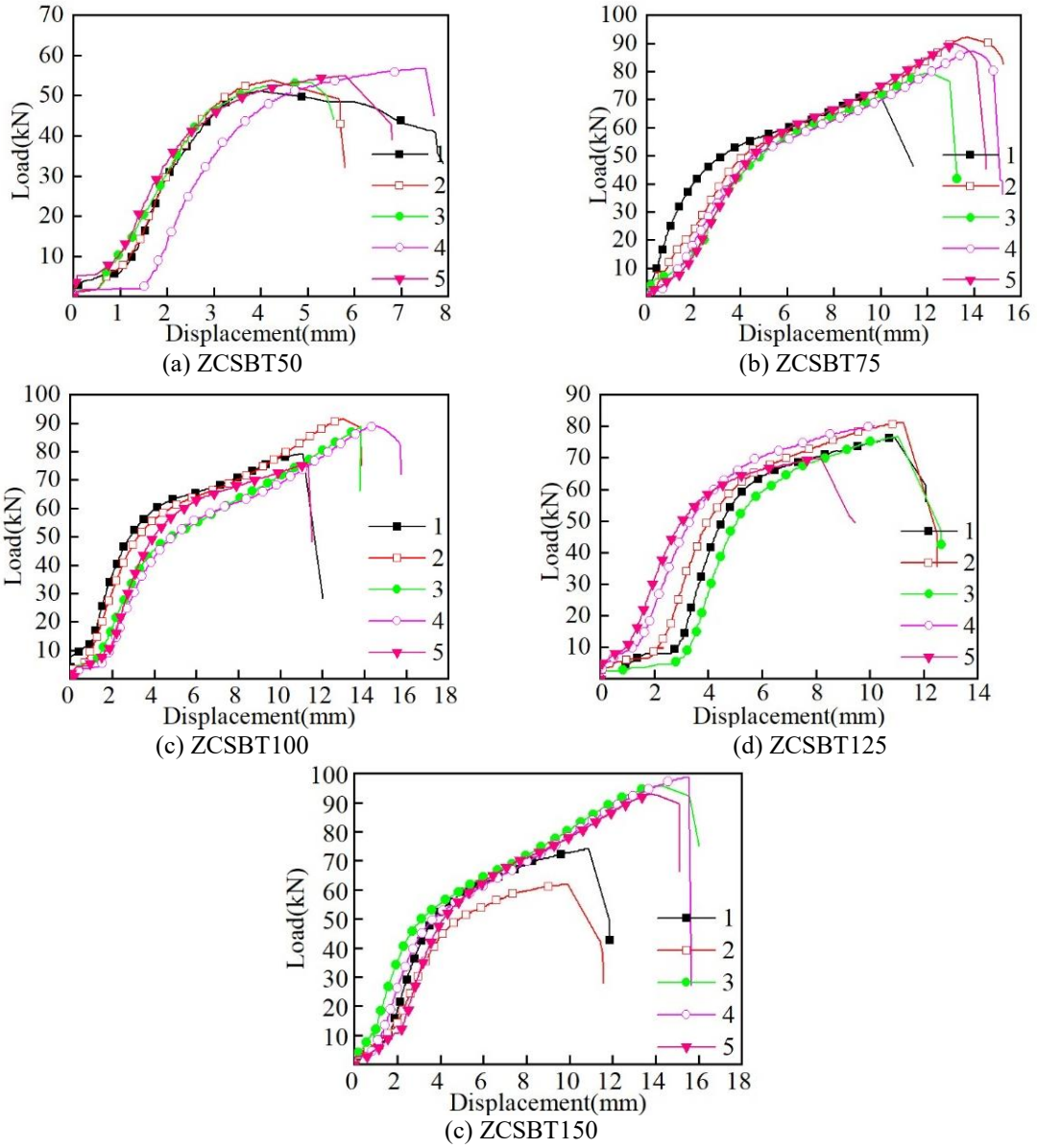

(a) ZCSBT50 (b) ZCSBT75

(c) ZCSBT100 (d) ZCSBT125

(c) ZCSBT150

Fig. 13. Load-slip curves of ZCSBT group

Fig. 13 shows the load-slip curve for ZCSBT group. Shear failure occurred directly to some specimens of ZCSBT50 series without secondary strengthening after reaching the ultimate load due to the thin size of the main component. The bolt for ZCSBT75, ZCSBT100, and ZCSBT125 series specimens bent with the load increasing after linear elastic stage. The stiffness decreased significantly, and there was an obvious yielding platform. After yielding, the bolt was subjected to secondary strengthening, when the connection displacement developed rapidly while the load developed slowly. The stiffness of the secondary strengthening was improved compared to the stiffness of the yielding stage but was significantly lower than the initial stiffness. The test results of each specimen of ZCSBT

group are shown in **Table. 4.**

Table 4 Test results of ZCSBT group

Number	P_y (kN)	d_y (mm)	K_1 (kN/mm)	K_2 (kN/mm)	P_u (kN)	d_u (mm)	μ	K_3 (kN/mm)
ZCSBT50-1	48.32	3.26	27.72	2.7	51.2	5.78	1.77	—
ZCSBT50-2	49.6	3.24	26.66	2.28	53.92	5.41	1.67	—
ZCSBT50-3	47.52	3.13	20.75	3.89	53.28	5.44	1.74	—
ZCSBT50-4	45.76	3.88	25.23	2.71	56.8	6.7	1.73	—
ZCSBT50-5	45.6	3.02	25.39	4.44	55.04	5.78	1.91	—
Average	47.36	3.31	25.15	3.204	54.05	5.82	1.76	—
CV	3.22%	9.05%	9.47%	28.6%	3.44%	8.97%	5.91%	
ZCSBT75-1	47.36	2.8	19.45	2.78	72.8	11.4	4.08	4.97
ZCSBT75-2	75.04	10.35	13.34	4.2	92.16	15.25	1.47	4.9
ZCSBT75-3	64.32	7.92	15.97	4.43	79.68	13.28	1.68	4.28
ZCSBT75-4	74.08	10.96	13.17	4.26	87.36	15.23	1.39	4.26
ZCSBT75-5	82.88	11.62	15.14	2.97	91.52	15.27	1.31	4.2
Average	68.74	8.73	15.41	3.728	84.7	14.08	1.99	4.522
CV	17.76%	36.88%	14.80%	21.1%	8.77%	10.97%	53.00%	8.38%
ZCSBT100-1	55.04	3.35	24.37	3.5	79.2	12.01	3.59	4.06
ZCSBT100-2	78.4	9.95	19.44	2.77	91.52	13.82	1.39	4.39
ZCSBT100-3	70.88	9.85	14.71	3.3	88.8	13.85	1.41	4.59
ZCSBT100-4	72.96	10.87	14.71	3.71	89.12	15.76	1.45	4.59
ZCSBT100-5	60.48	5.44	23.44	3.33	75.52	12.3	2.26	3.37
Average	67.55	7.89	19.33	3.322	84.83	13.55	2.02	4.2
CV	12.64%	37.42%	21.32%	10.51%	7.40%	9.89%	42.17%	12.19%
ZCSBT125-1	59.84	5.31	28.28	6.75	86.48	12.08	2.27	2.84
ZCSBT125-2	61.76	5.19	25.93	4.69	81.28	12.51	2.41	3.12
ZCSBT125-3	69.96	6.22	26.55	5.33	86.8	12.66	2.04	3.64
ZCSBT125-4	65.76	5.04	22.63	4.69	80.16	10.17	2.02	3.2
ZCSBT125-5	68.88	4.02	23.57	5.86	79.92	10.6	2.64	2.79
Average	67.24	5.15	25.39	5.464	82.93	11.6	2.28	3.118
CV	5.21%	13.65%	8.05%	15.92%	4.14%	8.80%	10.29%	10.92%
ZCSBT150-1	52.96	4.05	23.57	2.76	74.24	11.87	2.93	1.35
ZCSBT150-2	49.6	4.79	17.01	2.61	61.92	11.59	2.42	1..47
ZCSBT150-3	71.68	7.88	17.89	3.8	95.84	15.57	1.98	3.87
ZCSBT150-4	82.4	10.79	16.14	4.34	98.88	17.93	1.66	3.89
ZCSBT150-5	75.2	9.2	20.92	4.42	92.96	15.14	1.65	4.45
Average	66.37	7.34	19.11	3.586	84.77	14.42	2.13	3.39
CV	19.35%	35.00%	14.41%	23.93%	16.86%	16.62%	23.07%	40.89%

The influence of different thicknesses of main components on the stiffness, load and ductility ratio of nodes could be seen from **Fig. 14** and **Table. 4.** The initial stiffness of K_1 decreased significantly when the thickness of the main component increased from 50 mm to 75 mm and then increased as the thickness of the main component increased. The damage mode of ZCBT50 was shear damage, compared to ZCBT75 where the bolts did not yield when the main component was damaged. The initial stiffness reached a maximum value of 25.39 kN·m^{-1} for the main component with the thickness of 125 mm, and the data dispersion was small for the specimen with the main component with the thickness of 125 mm.

When the thickness of the main component reached 150 mm, the initial stiffness K_1 decreased again. The main reason might be that the thickness to the bolt diameter ration of the ZCSBT150 series

specimen was relatively large, resulting in the bolt yielding before the main member bolt hole damage, while the mechanical bearing capacity for the main component itself was not fully exploited. The effect of yield stiffness K_2 with the increased thickness of the main component was not obvious, where the maximum difference was only 2.2 kN·m^{-1}. The yield stiffness K_2 was less affected by the thickness of the main component. Therefore, under the premise of ensuring that the main member was not damaged by shear, i.e., the thickness of the main component should not be too small, the thickness of the main component was set at about 125 mm in order to give full play to the mechanical properties of the bolts and the main LBL component.

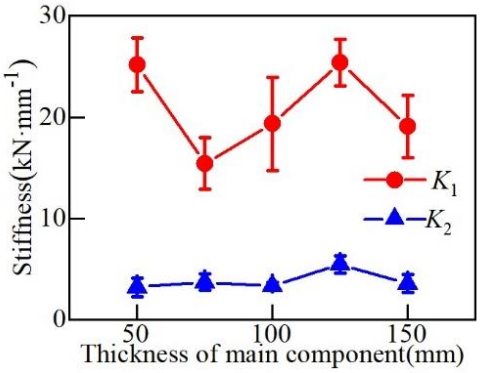

(a) Stiffness for different main member thicknesses

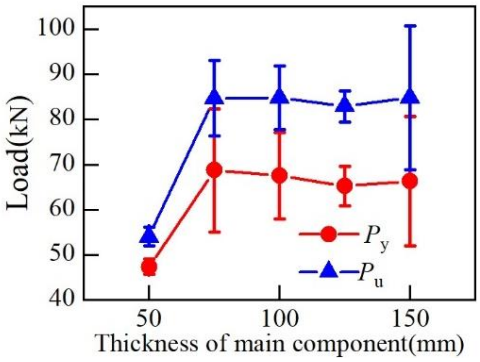

(b) Load for different main member thickness

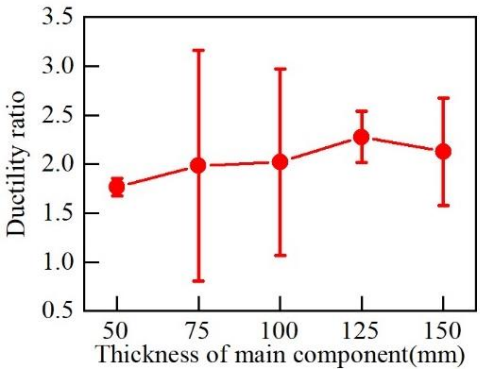

(c) Ductility ratio for different main member thicknesses

Fig. 14. Multiple comparisons of the different thicknesses of the main components

Fig. 14b shows that the yield load of ZCSBT50 series specimen is very small because the main component was sheared before the bolt yielded. As the shear damage occurred to the main component and the connection couldn't continue to carry, the difference between ultimate load and yield load was small. The yield load and ultimate load increased by 45.1% and 58.6%, respectively as the thickness of the main member increased to 75 mm. When the thickness of the main member continues to increase, the yield load and ultimate load do not change, where the load dispersion for ZCSBT125 series specimen is the smallest. It can be seen that the thickness of the main member has little effect on the load capacity of the connection if the shear damage does not occur before the bolt yields. That is, the influence of the thickness of the main component on the node bearing capacity is actually the influence of the bearing strength of the pin groove on the connection bearing capacity. When the main member meets the minimum size requirements, the pin groove bearing strength also basically tends to stabilize. Based on the above conclusions, it is recommended that the minimum size of the LBL-steel plate single-bolt connection nodes can be designed at 100 mm.

As can be seen from **Fig. 14c**, the ZCSBT50 series specimens have small plastic deformation and low ductility due to the brittle damage of the connections caused by the small thickness of the main member. As the thickness of the main component increased, the corresponding bolt length also increased. It leads to ductile failure under the combined action of the bolt and the main component and the connection could withstand greater plastic deformation. The ductility ratio increased to a maximum value of 2.28 until the thickness of the main component reached 125 mm, but there was a slight decrease in the ductility ratio when the thickness reached 150 mm. Therefore, when the thickness of LBL was

125mm, both the bolt and the main component could play their load-bearing performance well.

4.3 Effect of bolt end distance on node load-bearing performance

Fig. 15 shows the load-slip curves of ZCSBE60. A yield plateau could be seen clearly for the ZCSBE group series specimens at a load of about 60 kN. The connections of this series of specimens also showed the phenomenon of secondary strengthening after the end of the yielding phase. The stiffness at this point was smaller than the initial stiffness and slightly increased compared to the stiffness after yielding. The test results of each specimen of ZCSBE group are shown in **Table. 5.** The ZCSBE48 series has the same data as ZCSBT100 shown in **Table. 4**.

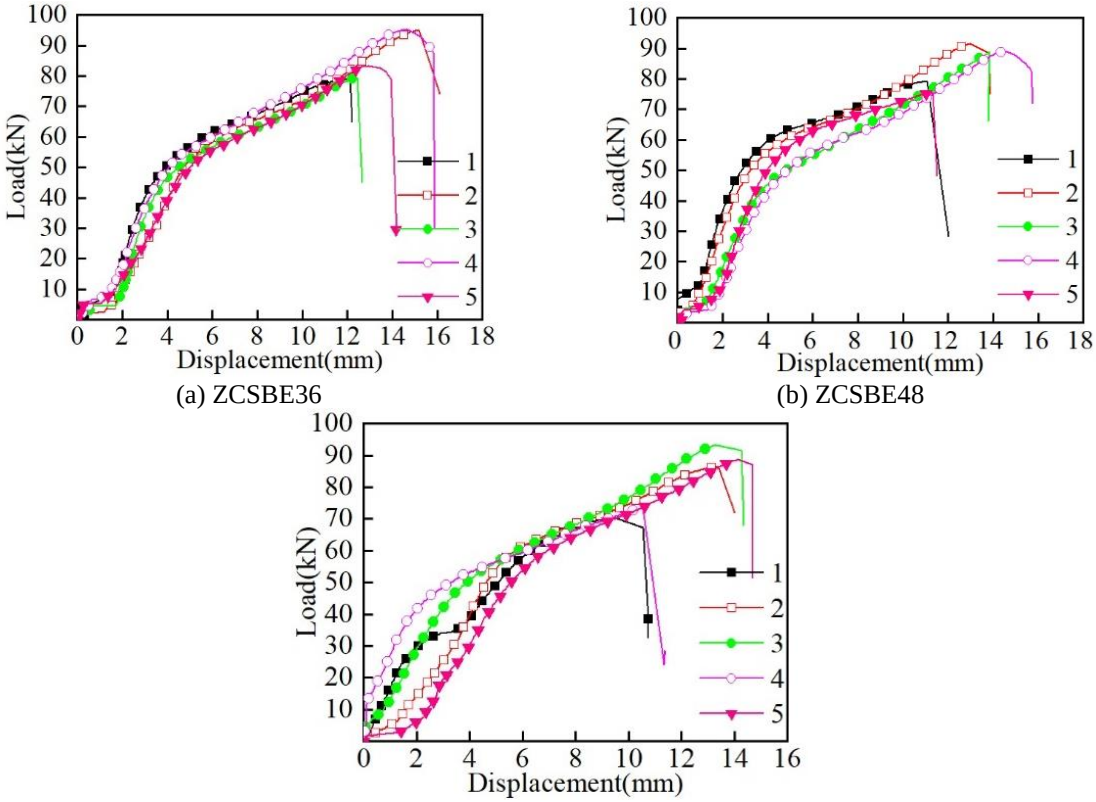

(a) ZCSBE36 (b) ZCSBE48

(c) ZCSBE60

Fig. 15. Load-slip curves of ZCSBE group

Table. 5. Test results of ZCSBE group

Number	P_y (kN)	d_y (mm)	K_1 (kN/mm)	K_2 (kN/mm)	P_u (kN)	d_u (mm)	μ	K_3 (kN/mm)
ZCSBE36-1	54.08	4.46	29.67	3.74	79.2	12.13	2.72	3.6
ZCSBE36-2	64.16	7.37	13.72	3.23	95.04	16.6	2.25	4.2
ZCSBE36-3	45.76	3.91	28.73	3.6	79.52	14.47	3.7	3.85
ZCSBE36-4	71.36	8.77	19.99	4	95.36	16.25	1.85	4.06
ZCSBE36-5	68.16	9.4	10.81	3.6	83.36	24.93	2.65	3.88
Average	60.7	6.78	20.58	3.63	86.5	16.87	2.64	3.918
CV	15.60%	32.85%	37.12%	7.67%	8.39%	25.66%	23.38%	5.80%
ZCSBE60-1	57.28	5.88	16.42	4.43	70.24	10.75	1.83	—
ZCSBE60-2	73.12	9.58	17.82	4.44	86.56	13.38	1.4	4.7
ZCSBE60-3	71.2	8.71	20.31	4	93.28	14.35	1.65	4.7
ZCSBE60-4	54.88	4.47	21.19	4.16	73.28	11.41	2.55	—
ZCSBE60-5	75.04	10.83	25.12	4.16	88.64	14.69	1.36	4.43
Average	66.3	7.89	20.17	4.24	82.4	12.91	1.76	4.61
CV	12.77%	29.91%	16.65%	4.52%	10.93%	12.18%	24.67%	3.38%

The effect of different bolt end distances on the stiffness, load, and ductility ratio of the connections can be seen from **Fig. 16** and **Table. 5.** The maximum and minimum initial stiffness is 20.58 kN·m^{-1}

and 19.33 kN·m^{-1} for ZCSBE36 and ZCSBE48 series, respectively, with the change of bolt end distance. The difference between the two is only 6.4%, which shows that the end distance has little effect on the initial stiffness of the node. Since the bolts were yielding at this point, the yield stiffness remained the same.

The effect of bolt end distance on the yield load of connection is shown in **Fig. 16b.** The yield load of the connection increases by 7 kN when the bolt end distance was increases from 36 mm to 48 mm, and there is no significant increase or decrease in the yield load when the end distance continues to increase. This shows that the effect of end distance on the yield load is insignificant as long as the end distance is too small before the bolt yields to avoid shear damage. And for the ultimate load with the increase of the end distance shows a slightly decreasing trend. The ultimate load is reduced by 4.7% when the end distance is increased from 3*D* (*D* is the bolt dimeter) to 6*D*. The ductility of the connection tends to decrease as the end distance increases, decreasing by 23.4% when the end distance increases from 3*D* to 4*D*, and then decreasing by 12.8% when it increases to 5*D*. When the end distance increases to 4*D*, the ductility rate does not change significantly when the end distance continues to increase in a more stable state. That is, increasing the end distance does not contribute substantially to the ductility ratio of the connection.

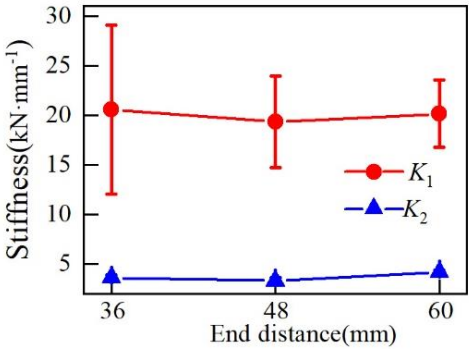

(a) Stiffness for different bolt end distance

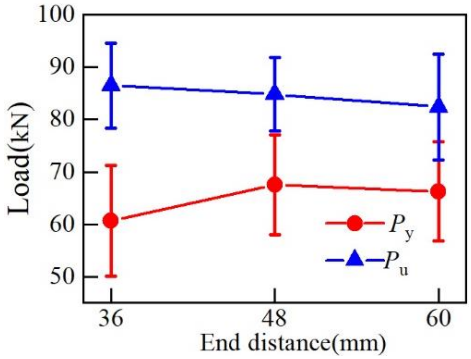

(b) Load for different bolt end distance

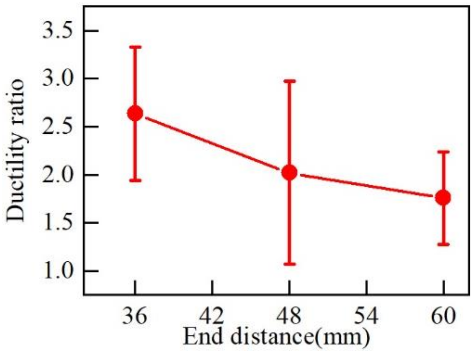

(c) Ductility ratio for different bolt end distance

Fig. 16. Multiple comparisons of the different bolt end distance

In summary, the load-bearing performance of the laminated bamboo lumber-steel plate single-bolt connection is influenced by the bolt diameter, the thickness of the main member, and the bolt end distance. When the bolt connection meets the minimum size design requirements, its load capacity mainly depends on the size of the bolt diameter. According to the above analysis, it is suggested that the minimum thickness of the main component and end distance of the single bolt connection of the LBL-steel plate are 100mm and 3*D*, respectively, at which time the bearing performance of the connection tends to be stable and the ductility rate reaches a better state.

5. Applicability of the current formula for timber bolt connection nodes

The design formulas for the load capacity of the bolted connections in the national design codes for wood structures are based on wood. The present study is based on laminated bamboo lumber, which is different from wood in terms of mechanical properties and structure. Therefore, by comparing the

theoretical and experimental values of the calculation formulae in different standard codes, the applicability of the calculation formulas of each standard for bolt connection in LBL is verified.

5.1 American wood structure design standards

Different failure mode will correspond to different formulas respectively. The mode I is mainly for the shear damage caused by the small thickness of the main component and the insufficient bonding force of the adhesive layer, the calculation formula is (1). Mode II is mainly due to the damage caused by insufficient bearing capacity of the pin groove, according to formula (2), to calculate the bolt connection bearing capacity. Mode III is mainly due to the bending deformation of the bolt caused by excessive extrusion deformation of the pin slot hole of the main component, connection shear damage, calculated according to Equation (3) [43].

$$Z = \frac{Dt_m F_{em}}{4K_\theta} \tag{1}$$

$$Z = \frac{Dt_s F_{em}}{1.6(2+R_e)K_\theta}\left[-1+\sqrt{\frac{2(1+R_e)}{R_e}+\frac{2F_{yb}(2+R_e)D^2}{3F_{em}t_m}}\right] \tag{2}$$

$$Z = \frac{D^2}{1.6K_\theta}\sqrt{\frac{2F_{em}F_{yb}}{3(1+R_e)}} \tag{3}$$

$$K_\theta = 1+\theta/360 \tag{4}$$

$$R_e = F_{em}/F_{es} \tag{5}$$

Where, Z is the bolt connection bearing capacity; t_m is the thickness of the main component; t_s is the thickness of the side component; F_{em} is the main component of the pin groove bearing strength; F_{es} is the compressive strength of the pin groove of the side component, the steel cleat used in this paper is taken as 590 MPa; F_{yb} is the bending strength of the bolt; D is the diameter of the bolt; θ is the maximum angle between the force and texture of any component in the connection, because of the existence of bending moment in the process of compression, so take 90 °.

5.2 European design standards for wood structures

According to Equation (6), to calculate the bearing capacity of the shear surface [44].

$$Z = \min\begin{cases} f_h t_m d \\ 4.6\sqrt{M_y f_h d} \end{cases} \tag{6}$$

Where, f_h is the characteristic value of compressive strength of paralleling pin groove; t_m is the thickness of the main component; d is the diameter of the bolt; M_y is the bolt yield bending moment.

5.3 Chinese design standards for wood structures

According to Equation (7), to calculate the bearing capacity of the shear surface [45].

$$Z = 2\times\min\begin{cases} \dfrac{\alpha\beta c d f_{hc}}{2} \\ \dfrac{c d f_{hc}}{\eta}\sqrt{\dfrac{1.647\beta f_{yk}}{3f_{ha}(1+\beta)}} \\ \dfrac{\beta c d f_{hc}}{2+\beta}\left[\sqrt{\dfrac{2(1+\beta)}{\beta}+\dfrac{1.647(2+\beta)f_{yk}}{3\beta f_{ha}\eta^2}}-1\right] \end{cases} \tag{7}$$

Where, $\alpha = c/a$, c and a are the thickness of the main component and side component respectively; $\beta = f_{hc}/f_{ha}$, f_{ha} and f_{hc} are the pin groove bearing strength of side component and main component

respectively; d is the bolt diameter; $\eta = a / d$ is the pin diameter ratio; f_{yk} is the bolt flexural yield strength.

The calculating results of the bearing capacity of the bolted connections for the above three standards are shown in **Table. 6** and **Fig. 17**. It can be seen that there are large deviations between the experimental values and the calculated values of different standards. The error between the calculated value and the test value of European and Chinese wood structure design standards is small. The calculated value of the American wood structure standard has a large error, and the calculated value is much smaller than the experimental value.

Table 6 Comparison of test values of different standard values

Group	5%yield test value	American Standard	Error	European Standards	Error	Chinese Standards	Error
ZCSBD12	72.44	27.86	61.54%	76.94	-6.21%	65.60	9.44%
ZCSBD14	83.16	37.92	54.40%	89.77	-7.95%	81.81	1.62%
ZCSBD16	98.68	49.53	49.81%	102.59	-3.96%	93.58	5.17%
ZCSBD18	126.43	62.69	50.42%	115.42	8.71%	119.33	5.61%
ZCSBD20	142.56	57.82	59.44%	128.24	10.04%	130.82	8.23%
ZCSBT50	47.36	19.24	59.38%	38.47	18.77%	32.80	30.74%
ZCSBT75	68.74	26.61	61.29%	57.71	16.05%	49.20	28.42%
ZCSBT100	67.55	24.33	63.98%	76.94	-13.90%	65.60	2.88%
ZCSBT125	67.24	22.87	65.98%	96.18	-43.04%	82.00	-21.96%
ZCSBT150	66.37	21.86	67.06%	115.42	-73.90%	98.40	-48.26%
ZCSBE36	60.7	24.33	59.92%	76.94	-26.75%	65.60	-8.08%
ZCSBE60	66.3	24.33	63.30%	76.94	-16.05%	65.60	1.05%

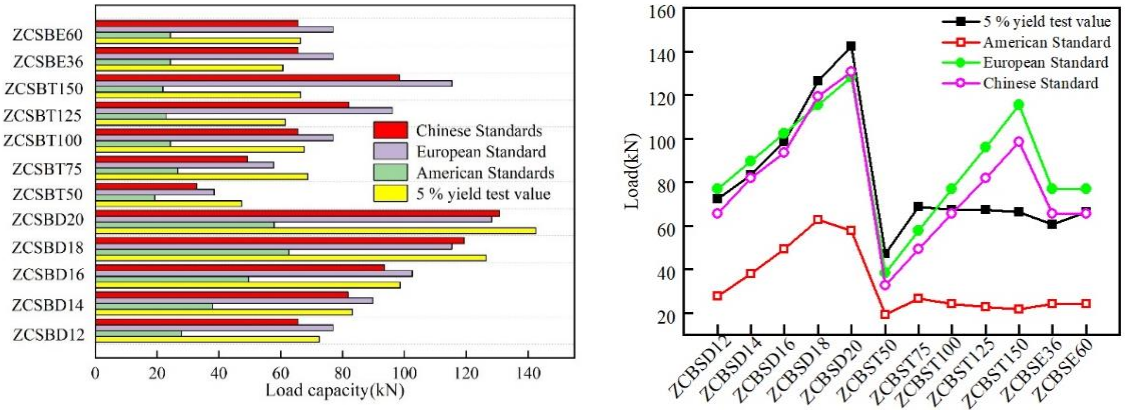

Fig. 17. Each specification standard and test value bearing capacity comparison

The calculation formula for single-bolt connections in the European standard for wood structure design takes into account the load-bearing strength of the pin groove as well as the influence of bolts. As the diameter increases, the load capacity of the single bolt connection node is affected by the bolt, which leads to a larger error when the bolt diameter is larger. Considering the thickness of the main component, the error is between -13.9% and 18.77% when the thickness is less than 125mm. As the thickness of the specimen increases, the error also increases. When the thickness increases to a certain extent, the influence of the thickness on the bearing capacity of the single-bolt connection decreases, and thus the error increases to more than 50%. Considering the bolt end distance of the specimen, the error between -13.9% and -26.75% is small. Overall, the calculated values of the European wood structure design standards are in good agreement with the test results. The calculation formula for single-bolt connections in the Chinese wood structure design standard not only takes into account the bearing strength of the pin groove, the diameter of the bolt, and the thickness of the main component, but also considers the pin diameter ratio, the bearing strength of the pin groove of the edge component, and the bending strength of the bolt. The theoretical values and experimental values show a high degree of agreement when the diameter and end distance are taken as influencing factors, with a maximum error of only 9.44%. When the thickness of the main component increases, the influence of thickness on the bearing capacity of the single-bolt connection decreases and reaches the optimal thickness at

125mm. Therefore, as the thickness of the main component continues to increase, the error gradually becomes larger.

Overall, the calculated values of the Chinese wood structure design standards have the highest degree of agreement with the test results. The theoretical calculation values of bolt connections in the American wood structure design standards all have errors of more than 50%, mainly because the American wood structure design standards adopt the allowable stress design method, and the safety factor is included in the bearing capacity calculation formula. This safety factor is jointly determined by the bearing strength and thickness of the pin grooves of the main components and side components, as well as the bending yield strength of the bolts. Meanwhile, the failure modes of the bolt connections are different, and the corresponding calculation methods are also different.

In summary, the prerequisite for using design specifications to predict connections is that the geometric construction features of the nodes meet the corresponding design requirements, and it is necessary to ensure as much as possible that the mechanical advantages of the connecting parts and main components can be maximized, so that the materials can be fully utilized.

5.4 Load-bearing capacity calculation formula for the LBL single-bolt connection nodes

As discussed above, the existing wood bolt connection load capacity design formula is not applicable to the main member thickness as the main influence of the LBL-steel plate single-bolt connection load capacity prediction. Therefore, adopting the design concept of single-bolt connection node bearing capacity in the Chinese Wood Structure Design Code and taking the influence of each factor on the single-bolt connection bearing capacity as the basis, the calculation formula of the single-bolt connection bearing capacity of LBL is proposed as follows:

$$N_v = k_v d^2 \sqrt{f_c} \tag{8}$$

where, N_v is the bearing capacity of each section of the single bolt connection; k_v is the calculation factor; d is the bolt diameter; f_c is the compressive strength of the material or the pin groove bearing strength.

As proved by the test, the bearing capacity of the connection is mainly affected by the bolt diameter and the thickness of the main component, so the bolt diameter and the thickness of the main component will be the main influencing factors. With $N_v / (d^2 \sqrt{f_c})$ as the vertical coordinate (where f_c is taken as the compressive strength of LBL and the compressive strength of LBL pin groove corresponding to different bolt diameters), the ratio of the thickness of the main component to the bolt diameter c/d is selected as the horizontal coordinate for fitting. The ultimate loads of the 8 groups of specimens with different c/d were taken as $2N_v$, and fitted with two kinds of strength values respectively as shown in **Fig. 18.**

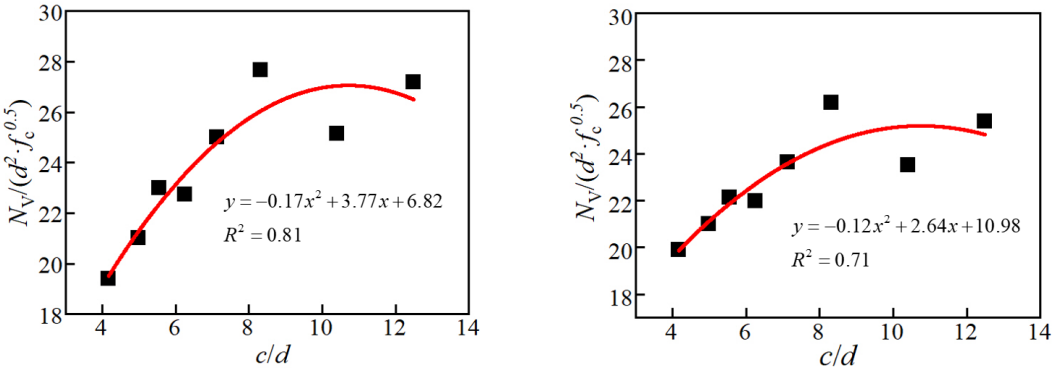

(a) Material compressive strength f_c (b) Pin groove pressure-bearing strength f_e

Fig. 18. Single bolt connection bearing capacity calculation coefficient

As can be seen from **Fig.18**, the coefficient of model evaluation (R^2) is 0.81 when f_c is taken as compressive strength and 0.71 when f_c is taken as the compressive strength of pin groove; the former

has a better agreement. Therefore, the compressive strength of LBL is taken as f_c for the pin slot bearing pressure of this paper. The calculation factor for the single bolt connection could be expressed as following:

$$k_v = -0.17(\frac{c}{d})^2 + 3.77 \times (\frac{c}{d}) + 6.82 \tag{9}$$

Equation (9) shows that the calculation coefficient is mainly related to the thickness of the main LBL component and bolt diameter. Substitute formula (9) into the calculation formula (8) for calculating the bearing capacity of single bolt connection. After simplifying, the theoretical calculation formula of the bearing capacity for each section of the LBL-steel plate single-bolt connection could be expressed as follows:

$$N_v = (-0.17c^2 + 3.77cd + 6.82d^2)\sqrt{f_c} \tag{10}$$

Where, N_v is the bearing capacity of each section of the single bolt connection; c is the thickness of the main component; d is the diameter of the bolt; f_c is the compressive strength of the LBL.

Table. 7. Comparison between the test value and the calculated value for the bearing capacity

	Test value	Fitted value	error
ZCSBD12	72.44	64.57	-11%
ZCSBD14	83.16	83.38	0%
ZCSBD16	98.68	103.11	4%
ZCSBD18	126.43	123.77	-2%
ZCSBD20	142.56	145.35	2%
ZCSBT50	47.36	47.82	1%
ZCSBT75	68.74	58.00	-16%
ZCSBT100	67.55	64.57	-4%
ZCSBT125	67.24	67.53	0%
ZCSBT150	66.37	66.89	1%
ZCSBE36	60.7	64.57	6%
ZCSBE60	66.3	64.57	-3%

As shown in **Table. 7,** the calculated results of the semi-empirical formula are in good consistent with the experimental results. Therefore, Equation (10) can give a reference for calculating the bearing capacity of the LBL-steel plate single-bolt connections.

6 Conclusions

This mechanical properties of the LBL-steel plate single-bolt connections were investigated under compression parallel to grain, considering the bolt diameter, the thickness of the main component and bolt end distance. The following conclusions were drawn:

(1) The failure modes of the single-bolt connections of the LBL could be divided into three main categories: shear damage, one hinge yielding, and two hinge yielding mode. With the increase of the thickness to diameter ratio (main component thickness/bolt diameter), the damage mode of the connections changed gradually from shear damage to yielding damage.

(2) The load displacement curve of the connection had a small free slip in the initial stage when the bolt was not in contact with the main component, and the load displacement curve of the connection entered the linear elastic stage after complete contact. As the sliding displacement of the connection gradually increased, the bolt was gradually embedded into the main components, and the linear elastic stage ended and entered the yield stage. At this time, the bolt gradually bent with the increased load, the connection stiffness decreased significantly. There was an obvious yielding platform, and some specimens underwent second reinforcement after yielding.

(3) The influence of bolt diameter on the bearing capacity of connections is as follows: as the bolt diameter increases, the initial stiffness and bearing capacity of the connection increase gradually. However, for the ductility ratio of the connection, when the bolt diameter increased to 16 mm, the ductility ratio of the connection no longer increased with the increase of bolt diameters. Therefore, when

the bolt diameter was around 16 to 18mm, the ductility ratio of the node reached its maximum value, and the load-bearing performance of the bolt and the main component was fully utilized at this time.

(4) The initial stiffness of the connections reached the maximum value at 125 mm thickness of the main component under the premise of ensuring that the thickness of the main component was too small to be damaged by shear. The yield load and ultimate load no longer showed a significant increasing trend when the thickness reached 100mm. The ductility ratio was less affected by the thickness of the main component than the bolt diameter, and there was no significant changing trend with the increase of the main component thickness. When the main component thickness reached 125mm, the ductility ratio reached the maximum value of 2.28. That is to say, when the thickness of the main component was 125mm, both the bolts and the main component can exert their own load-bearing performance well.

(5) The influence of the end spacing on the initial stiffness, yield load and ultimate load of the connection was far less than that of the bolt diameter and the thickness of the main component on them. That was, as the end spacing increased, neither the stiffness nor the load showed a significant changing trend. As for the ductility ratio, it reached the maximum value when the bolt end spacing was 3*D*.

(6) Both Chinese and European wood structure design standards have good consistency with the test values. The calculated values of the American wood structure design standards are much lower than the test values, which is overly conservative. Considering the bolt diameter and the thickness of the main component as the main influencing factors, the load capacity calculation formula of the connections was proposed and compared with the test results. The formula could give a reference for the calculation of the load capacity of the LBL-steel plate single-bolt connections.

Acknowledgement

The writers gratefully acknowledge Dong Yang, Han Zhang and others from the Nanjing Forestry University for assisting in various capacities.

Funding Statement

This work was supported by the National Natural Science Foundation of China (No. 51878354 & 51308301); the Natural Science Foundation of Jiangsu Province (No. BK20181402 & BK20130978); 333 high-level talent project of Jiang-su Province; and Qinglan Project of Jiangsu Higher Education Institutions. All research outcomes presented in this paper are those of the writer(s) and do not necessarily reflect the views of the foundations.

CRediT authorship contribution statement

Jingwen Su: Investigation, Formal analysis, Writing – original draft. **Yukun Tian**: Investigation, Formal analysis, Writing – original draft. **Yijia Guo**: Investigation, Formal analysis, Writing – original draft. **Haitao Li**: Conceptualization, Funding acquisition, Supervision, Investigation, Formal analysis, Writing – original draft. **Zhenhua Xiong**: Supervision, Writing – review & editing. **Usama Sayed**: Investigation. **Gensheng Cheng**: Supervision, Investigation. **Rodolfo Lorenzo**: Investigation, Writing – review & editing.

Conflicts of Interest

The authors declare that they have no conflicts of interest in this work.

Data Availability Statement

The authors declare that they have no conflicts of interest to report regarding the present study.

References

[1] Sun, X., He, M., Li, Z. Novel engineered wood and bamboo composites for structural applications: state-of-art of manufacturing technology and mechanical performance evaluation. *Construction and Building Materials* 2020; 249: 118751. https://doi.org/10.1016/j.conbuildmat.2020.118751

[2] Hu Y A, Huang H, He L, et al. Research status and development trends of “bamboo as as ubstitute for plastic”

in construction and building materials. *Journal of Forestry Engineering* 2024; 9(6): 1-11. https://doi.org/10.13360/j.issn.2096-1359.202408029.

[3] Li, H., Luo, Y., Guo, Y., Tian, Y., Zhou, C., Lorenzo, R.. Mechanical properties of bamboo scrimber under bolted connections with steel splints. *Sustainable Structures* 2025; 5(4): 000091. https://doi.org/10.54113/j.sust.2025.000091

[4] Lorenzo, R., Mimendi, L., Godina, M., Li, H. Digital analysis of the geometric variability of Guadua, Moso and Oldhamii bamboo. *Construction and Building Materials* 2020; 236: 117535. https://doi.org/10.1016/j.conbuildmat.2020.120876

[5] Huang, M., Zhang, X., Yu, W., Li, W., Liu, X., Zhang, W. Mechanical properties and structure characterization of bamboo softened by high temperature steam. *Journal of Forestry Engineering* 2016; 1(4): 64-68. https://doi.org/10.13360/j.issn.2096-1359.2016.04.010

[6] He, W., Song, J.G., Wang, T., Li, J.S., Xie, L.X., Yang, Y., Wu, B., Zhang, Q.S. Effect of heat oil treatment on bamboo scrimber properties. *Journal of Forestry Engineering* 2017; 2(5): 15-19. https://doi.org/10.13360/j.issn.2096-1359.2017.05.003

[7] Li, H., Wu, G., Xiong, Z., Corbi, I., Corbi, O., Xiong, X., Zhang，H., Z, Qiu. Length and orientation direction effect on static bending properties of laminated moso bamboo. *Holz als Roh- und Werkstoff* 2019: 77(4): 547-557. https://doi.org/10.1007/s00107-019-01419-6

[8] Chen, G., Yu, Y.F., Li, X., He, B. Mechanical behavior of laminated bamboo lumber for structural application: an experimental investigation. *European Journal of Wood and Wood Products* 2020; 78(1): 53-63. https://doi.org/10.1007/s00107-019-01486-9

[9] Li, H.T., Zhang, Q.S., Huang, D.S., Deeks, A.J. Compressive performance of laminated bamboo. *Composites Part B: Engineering* 2013; 54: 319-328. http://doi.org/10.1016/j.compositesb.2013.05.035

[10] Mahdavi, M., Clouston, P. L., Arwade, S. R. Development of laminated bamboo lumber: review of processing, performance, and economical considerations. *Journal of materials in Civil Engineering* 2011; 23(7): 1036-1042. https://doi.org/10.1061/(ASCE)MT.1943-5533.0000253

[11] Wang, Z., Li, H., Yang, D., Xiong, Z., Sayed, U., Lorenzo, R., Hong, C. Bamboo node effect on the tensile properties of side press-laminated bamboo lumber. *Wood Science and Technology* 2021; 55(1): 195-214. 10.1007/s00226-020-01251-9

[12] Zhang, H., Li, H., Hong, C., Xiong, Z., Lorenzo, R., Corbi, I., & Corbi, O. Size effect on the compressive strength of laminated bamboo lumber. *Journal of Materials in Civil Engineering* 2021; 33(7): 04021161. https://doi.org/10.1061/(ASCE)MT.1943-5533.0003776

[13] Zhang, H., Li, H., Li, Y., Xiong, Z., Zhang, N., Lorenzo, R., & Ashraf, M. Effect of nodes on mechanical properties and microstructure of laminated bamboo lumber units. *Construction and Building Materials* 2019; 304: 124427. https://doi.org/10.1016/j.conbuildmat.2021.124427

[14] Li, H. T., Liu, R., Lorenzo, R., Wu, G., Wang, L. B. Eccentric compression properties of laminated bamboo columns with different slenderness ratios. *Structures & Buildings* 2019; 172(5): 315-326. https://doi.org/10.1680/jstbu.18.00007

[15] Li, H., Yang, D., Chen, B., Mohrmann, S., Lorenzo, R., Zhou, K., Shen, F.. Flexural performance of prestressed reinforced laminated bamboo lumber beams with GFRP bars. *Sustainable Structures* 2025, 5(1): 000070. https://doi.org/10.54113/j.sust.2025.000070.

[16] Lei, J., Chen, B., Yuan, P. Experimental study on flexural properties of side-pressure laminated bamboo beams. *Advances in Civil Engineering* 2020; (4): 1-10. https://doi.org/10.1155/2020/5629635

[17] Li, H., Wu, G., Zhang, Q.S., Deeks, A.J., Su, J. Ultimate bending capacity evaluation of laminated bamboo lumber beams. *Construction & Building Materials* 2018; 160(JAN.30): 365-375. https://doi.org/10.1016/j.conbuildmat.2017.11.058

[18] Li, H.T. Chen, B., Fei, B.H., Li, H., Xiong, Z.H., Lorenzo, R., Fang, C.H., Ashraf, M. Mechanical properties of aramid fiber reinforced polymer confined laminated bamboo lumber column under cyclic loading. *European Journal of Wood and Wood Products* 2022; 80: 1057-1070. https://doi.org/10.1007/s00107-022-01816-4

[19] Sinha, A., Way, D., Mlasko, S. Structural performance of glued laminated bamboo beams. *Journal of Structural Engineering* 2014; 140(1): 896-912. https://doi.org/10.1061/(ASCE)ST.1943-541X.0000807

[20] Li, H., Li, H.T., Hong, C.K., Xiong, Z., Lorenzo, R., Corbi, I., Corbi, O. Experimental investigation on axial compression behavior of laminated bamboo lumber short columns confined with CFRP. *Composites Part A: Applied Science and Manufacturing* 2021; 150: 106605. https://doi.org/10.1016/j.compositesa.2021.106605

[21] Hong, C., Li, H., Xiong, Z., Lorenzo, R., Corbi, I., Corbi, O. Experimental and numerical study on eccentric compression properties of laminated bamboo columns with a chamfered section. *Journal of Building Engineering* 2021; 43: 102901. https://doi.org/10.1016/j.jobe.2021.102901

[22] Hong, C., Li, H., Xiong, Z., Lorenzo, R., Li, X., Wang, Z. Axial compressive behavior of laminated bamboo lumber columns with a chamfered section. *Structures* 2021; 33: 678-692. https://doi.org/10.1016/j.istruc.20

21.04.083
[23] Li, H.T., Su, J.W., Zhang, Q.S., Deeks, A.J., Hui, D. Mechanical performance of laminated bamboo column under axial compression. *Composites part B: engineering* 2015; 79: 374-382. https://doi.org/10.1016/j.compositesb.2015.04.027
[24] Hong, C.K., Li, H., Lorenzo, R., Wu, G., Zhang, H. Review on Connections for Original Bamboo Structures. *Journal of Renewable Materials* 2019; 7(8): 713-730. https://doi.org/10.32604/jrm.2019.07647
[25] Hong, C.K., Li, H.T., Xiong, Z.H., Lorenzo, R., Corbi, I., Corbi, O., Wei, D.D., Yuan, C.G., Yang, D., Zhang, H.Z. Review of connections for engineered bamboo structures. *Journal of Building Engineering* 2020; 30: https://doi.org/101324. 10.1016/j.jobe.2020.101324
[26] Trayer, G. W. The bearing strength of wood under bolts. *US Department of Agriculture*. 1932.
[27] Johansen, K. Theory of timber connection. *International Association for Bridge & Structural Engineering* 9.
[28] McLain, T. E., & Thangjitham, S. Bolted wood-joint yield model. *Journal of Structural Engineering* 1983; 109(8): 1820-1835. https://doi.org/10.1061/(ASCE)0733-9445(1983)109:8(1820)
[29] Soltis, L. A., Hubbard, F. K., & Wilkinson, T. L. Bearing strength of bolted timber joints. *Journal of Structural Engineering* 1986; 112(9): 2141-2154. https://doi.org/10.1061/(ASCE)0733-9445(1986)112:9(2141)
[30] Gattesco, N., Toffolo, I. Experimental study on multiple-bolt steel-to-timber tension joints. *Materials & Structures* 2004; 37(2): 129-138. https://doi.org/10.1007/BF02486609
[31] Cesar, E. Capacity predictions for bolted timber joints failing by split-ting. In Proceedings of the World Conference on Timber Engineering, Miyazaki, Japan 2008; 2-5.
[32] Li, X., Zhong, Y., Ren, H. Review on performance and impact factors of bolted connection in modern wood structure. *World Forestry Research* 2012; 25(4): 52-57. https://doi.org/10.13348/j.cnki.sjlyyj.2012.04.004
[33] Meghlat, E. M., Oudjene, M., Ait-Aider, H., Batoz, J. L. A new approach to model nailed and screwed timber joints using the finite element method. *Construction and Building Materials* 2013; 41: 263-269. https://doi.org/10.1016/j.conbuildmat.2012.11.068
[34] Lokaj, A., Klajmonová, K. Round timber bolted joints exposed to static and dynamic loading. *Wood research* 2014; 59(3): 439-448.
[35] Zhu, E., Pan, J., Zhou, X., Zhou, H. Experiments of load-carrying capacity of bolted connections in timber structures and determination of design value. *Journal of Building Structures* 2016; 37(04): 54-63. https://doi.org/10.14006/j.jzjgxb.2016.04.008
[36] Meghlat, E. M., Oudjene, M., Ait-Aider, H., & Batoz, J. L. A new approach to model nailed and screwed timber joints using the finite element method. *Construction and Building Materials* 2013; 41: 263-269. https://doi.org/10.1016/j.conbuildmat.2012.11.068
[37] Thomas, R., Bhavna, S., Kent, H., Michael, R. Dowelled structural connections in laminated bamboo and timber. *Composites Part B Engineering* 2016; 90: 232-240. https://doi.org/10.1016/j.compositesb.2015.11.045
[38] Zhou A,P., Huang D.S., Tang, S.Y., Zhao, S.Y. Experimental research on bearing capacity of the bolted PSB-steel-PSB joints. *Journal of Nanjing Tech University* 2016; 38(5): 34-39+67. https://doi.org/10.3969/j.issn.1671-7627.2016.05.006
[39] Khoshbakht, N., Clouston, P. L., Arwade, S. R., Schreyer, A. C. Computational modeling of laminated veneer bamboo dowel connections. *Journal of Materials in Civil Engineering* 2016; 30(2): 04017285. https://doi.org/10.1061/(ASCE)MT.1943-5533.0002135
[40] Cui, Z.Y., Xu M., Chen Z.F., Wang, F. Experimental study on bearing capacity of bolted steel-psb-steel connections. *Engineering mechanics* 2019; 36(1): 96-103+118. https://doi.org/10.6052/j.issn.1000-4750.2017.11.0792
[41] Li X.Z., Ren H.Q., Li X.J., Zhong Y., Xu, K., Hao X.F. The Bearing Properties and Failure Mode of Bolted Steel-Bamboo Scrimber-Steel Connections. *Scientia Sivae Sinicae* 2021; 57(08): 157-166. https://doi.org/10.11707/j.1001-7488.20210816
[42] American Society for Testing and Materials. Standard test method for evaluating dowel-bearing strength of wood and wood-based products. ASTM International, 2007.
[43] ANSI/AWC (American National Standards Institute/American Wood Council). National design specifications (NDS) for wood construction. 2015.
[44] Steer, P. J. EN1995 Eurocode 5: Design of timber structures. *Proceedings of the Institution of Civil Engineers-Civil Engineering*. Thomas Telford Ltd, 2001; 144(6): 39-43. https://doi.org/10.1680/cien.2001.144.6.39
[45] Ministry of Construction of the People's Republic of China. Code for the design of wood structures (GB50005-2017). Beijing: China Construction Industry Press, 2017.